EXPERIMENTAL VALIDATION OF THE PREDICTED EMERGENT MAGNETISM IN DIAMAGNETIC CADMIUM SULFIDE (CdS) DOPED WITH BORON

by

Bilal Azhar

Submitted to the
Department of Materials Science and Engineering
in Partial Fulfillment of the Requirements for the Degree of

Bachelors of Science

at the

Massachusetts Institute of Technology

May 2020

Signature of Author……
Department of Materials Science and Engineering
May 10, 2020

Certified By……
Rafael Jaramillo
Assistant Professor of Materials Science and Engineering
Thesis Supervisor

Accepted By……
Juejun Hu
Associate Professor of Materials Science and Engineering
Chair, DMSE Undergraduate Thesis Committee

TABLE OF CONTENTS

EXPERIMENTAL VALIDATION OF THE PREDICTED EMERGENT MAGNETISM IN DIAMAGNETIC CADMIUM SULFIDE (CdS) DOPED WITH BORON

Bilal Azhar, Rafael Jaramillo

ABSTRACT

The large and persistent photoconductivity displayed by some semiconductors provides a way to control magnetism with light, through illumination-control of free carrier concentration and thereby magnetic interaction in dilute magnetic semiconductors. CdS is a wide band-gap semiconductor that displays large and persistent photoconductivity and is predicted to become magnetic when doped with certain dopants such as Boron[1]. In this work, we experimentally test the prediction of magnetic CdS:B, and lay groundwork for testing the hypothesis that magnetism can be controlled by photoconductivity. We make CdS:B nanoparticles by co-precipitation[2]. We use X-ray diffraction and plasma optical emission spectroscopy to quantify boron doping. We use magnetometry to confirm the presence of magnetic B.

BACKGROUND

Introduction

Semiconductor devices take advantage of electronic charge for information processing applications and magnetic materials take advantage of electron spin for memory storage applications. Dilute Magnetic Semiconductors (DMS) exhibit spin-charge coupling which holds potential for simultaneous information processing and memory storage[1]. Thus, DMS hold potential for spintronics research, which investigates spin-based systems for a superior alternative to traditional electronic systems in information technology applications[3].

The use of a magnetic dopant in traditional DMS presents obstacles in magnetic characterization. The magnetic signal from the aggregates and secondary phases interferes with the desired magnetic signal from the lattice-incorporated dopant sites[4]. In this thesis, **we report a new type of DMS by confirming the theoretical prediction of emergent magnetic behavior in diamagnetic CdS doped with boron**[1]. The use of a non-magnetic dopant will limit magnetic behavior to lattice sites with a successfully incorporated boron atom, and thereby suppress magnetic interference from aggregates or secondary phases.

We will also set the groundwork for a future investigation of the fundamental relationship between photoconductivity and magnetism in DMS, for the development of an illumination-based control mechanism for the spin-charge coupling in DMS. We hypothesize that by taking advantage of CdS's large and persistent photoconductivity[5] we can control its new-found emergent-magnetism with light, via illumination-control of the free carrier concentration and thereby the magnetic interaction in DMS.

Dilute Magnetic Semiconductors

Dilute Magnetic Semiconductors (DMS) are semiconductors that exhibit magnetic behavior upon being doped with a magnetic element. The magnetic dopant substitutes into randomly distributed lattice sites within the semiconductor matrix, where it behaves as a donor or an acceptor and introduces a localized spin and free charge carrier[3]. This can be seen in Figure 1 where the magnetic dopant substitutes into the lattice at the triangle lattice sites and introduces a local spin. The spins act as localized magnetic moments, and the interaction between these localized magnetic moments and free carriers determines the larger magnetic behavior of the semiconductor[6].

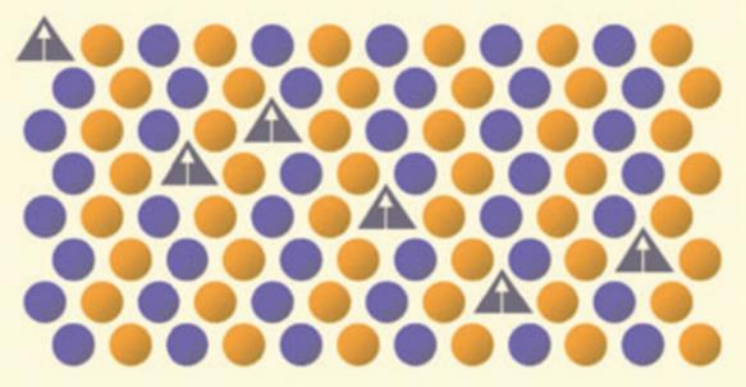

Figure 1: The (Ga,Mn)As DMS where Mn^{2+} substitutes for Ga (purple) at randomly distributed lattice sites (triangles) which have a local magnetic moment represented by an arrow. Image reproduced from[3].

The exact exchange mechanisms are still debated, and as such there is no general model that predicts the resultant magnetic behavior of the semiconductor[6]. However, it is commonly accepted that the interactions between the local magnetic moments are carrier-mediated as described by the mean-field Zener Model. According to the Zener model, the system lowers its energy by ordering the localized magnetic moments via coupling of the localized spin with the

spin of the surrounding carriers[7]. Due to this spin-carrier coupling, an external magnetic field-induced alignment of the localized spins leads to the subsequent alignment of the carrier spins, which produces a larger magnetic response in the semiconductor.

The Zener model is a simpler version of the RKKY model which, unlike the Zener model, factors for the sign oscillations, or Friedel oscillations, of the interaction between the localized spins with respect to spin-spin distance[7]. However, in DMS the effect of the Friedel oscillations can be neglected since the distance between the Friedel oscillations is much greater than the average distance between localized spins[7].

Theoretical Prediction of Emergent Magnetism from Doping Diamagnetic CdS with a Non-Magnetic Element

Bedolla et al. used ab initio density functional theory (DFT) methods to predict that doping diamagnetic CdS with certain non-magnetic elements will induce paramagnetism and possible long-range order[1]. Bedolla et al. performed separate calculations for the zincblende (cubic) structure and the wurtzite (hexagonal) structure, and found no significant difference due to the structural variation[1]. They modeled a high concentration 16-atom cell and a lower concentration 64-atom cell, in which the impurity substituted a sulfur atom, to study three major interactions: (i) interaction between the impurities, (ii) interaction between the impurity and the nearest neighbor (NN), and (iii) interaction between the impurity and the next nearest neighbor (NNN)[1]. Figure 2 compares the 16-atom cell (top) and 64-atom cell (bottom). The above interactions suppress magnetic behavior and are weakened by a decrease in concentration; thus, we observe a general increase in magnetic moments from the 16-atom cell to the 64-atom cell in Figure 2[1]. C, Si, and Ge each introduce two holes such that the Fermi energy, of their non-

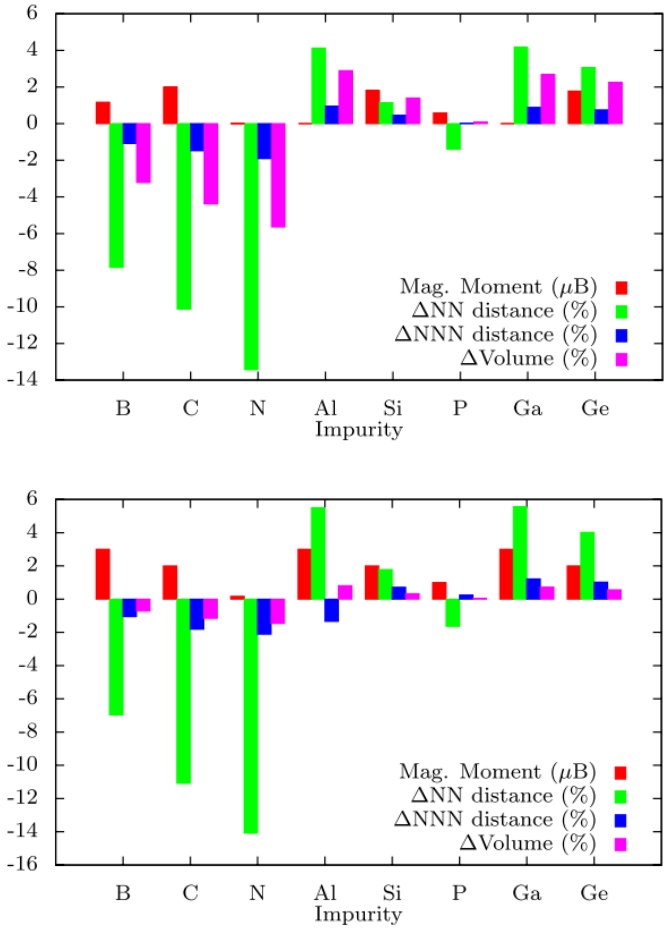

Figure 2: (top) high-concentration 16-atom zincblende cell (bottom) low-concentration 64-atom zincblende cell. Image reproduced from[1].

magnetic state, is at a large-enough density of states peak that fulfils the Stoner criterion and magnetically splits the p-bands; thus, leaving them saturated which is observed by the lack of change in their magnetic moments in Figure 2[1]. B, Al, and Ga experience stronger interactions with other impurities, (i), due to their large wavefunctions, and experience an increase in their magnetic moments with a decrease in the (i) interaction in Figure 2[1]. N and P experience a strong interaction with their NN, (ii), which does not weaken sufficiently enough for their magnetic moments to increase in Figure 2[1].

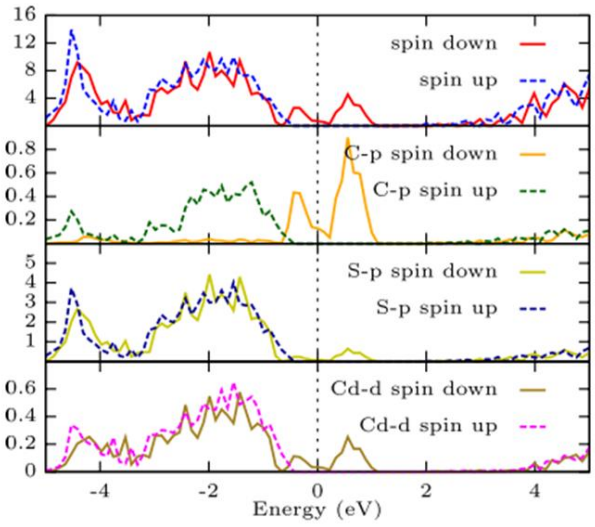

Figure 3: Density of States for the 16-atom carbon-doped zincblende supercell. Image reproduced from[1].

The impurities exhibit half-metallic behavior which can explain the predicted emergent magnetic behavior. The coupling between the impurity p-orbitals, the sulfur p-orbitals, and cadmium d-orbitals produces states "that sit at the Fermi energy in the spin-down channel and extend over the whole Brillouin zone, while a gap remains in the spin-up channel[1]." The DOS for the carbon-doped system, which resembles the DOS of the other impurities, in Figure 3 shows clear half-metallic behavior with a gap in the spin-up side.

Since we were uncertain about what concentration to expect in our samples, we decided to choose an element with a high magnetic moment even in the 16-atom cell. From B, C, Si, and Ge we choose to test boron because synthesis of B-doped CdS was more established the others.

Optical Control of DMS

Using illumination as a control mechanism for the spin-charge coupling in DMS could allow the integration of electronic, magnetic, and photonic degrees of freedom in future spintronic devices. It is well known that the free electron concentration in CdS varies over many orders of magnitude with illumination due to its giant photoconductive effect[5]. CdS also has persistent photoconductivity where it has a low decay rate of its photogenerated carrier concentration upon the removal of illumination. The magnetic behavior of a DMS is from the combined summation of its free carrier spins and impurity spins. In theory, an increase in the free carrier concentration of a DMS would also cause an increase in its magnetization. Therefore, we hypothesize that by controlling the free carrier concentration of CdS via photoconductivity (or simply illumination), we can also control its magnetic behavior. CdS's large and persistent photoconductivity gives it the advantage of being able to observe a strong response and to maintain that response for longer. Being a wide bandgap semiconductor, CdS will observe less noise and have clear distinction between the low-free-carrier-concentration/low-magnetization state and the high-free-carrier-concentration/high-magnetization state.

Previous work has had success with using illumination-controlled free carrier concentration to influence the magnetic behavior of DMS. Wang et al. demonstrated enhancement of ferromagnetism in GaMnAs via photoexcited holes[8]. Figure 4a shows ferromagnetic enhancement under illumination with the shifting of the Curie temperature, T_c, to the right[8]. The magnetic enhancement is also shown by the MOKE profile in Figure 4c, where initial demagnetization behavior is observed followed by a magnetic enhancement[8]. The initial drop is due to the spin scattering of the hot holes, excited holes that can overcome interfaces,

formed by initial photoexcitation[8]. The magnetic enhancement observed in Figure 4a and 4c is due to the increased ferromagnetic exchange mediated by the illumination-created holes in the GaMnAs valence band in Figure 4b.

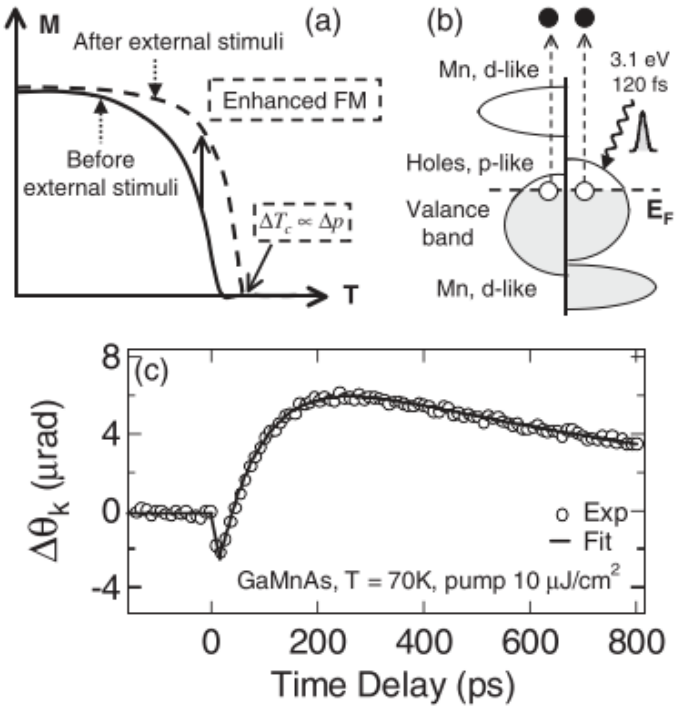

Figure 4: (a) Magnetization vs. Temperature curve showing enhanced ferromagnetic behavior under external illumination stimuli and increase in the Curie temperature T_c (b) Illumination creates large density of holes in the GaMnAs valence band (c) Time-resolved MOKE dynamics showing general magnetic enhancement over time under illumination. Image reproduced from[8].

Koshihara et al. observed an illumination-induced paramagnetic to ferromagnetic transition in a DMS heterojunction[9]. They observed a long lasting ferromagnetic transition due to persistent photoconductivity as seen in Figure 5[9]. The DMS was cooled to 5K, in dark, where it was irradiated for 30 min, followed by a 20 min rest in the dark; then, it was warmed under a magnetic field of 0.02 T, Figure 5[9]. The under-dark cooling-behavior (open circles) was paramagnetic as supported by the Curie-Weiss plot in the inset[9]. However, the subsequent

post-irradiation warming-behavior was ferromagnetic; with the system upholding the ferromagnetic transition until 35 K, in the absence of irradiation[9]. The preservation of ferromagnetic order in the absence of irradiation is due to the persistent photoconductivity[9]. The phase transition was induced by the increased ferromagnetic spin exchange caused by the photogenerated carriers[9]. Koshihara et al. observed this transition with only a 6% increase in conductivity which hints to the sensitivity of the magnetic ordering to carrier concentration[9].

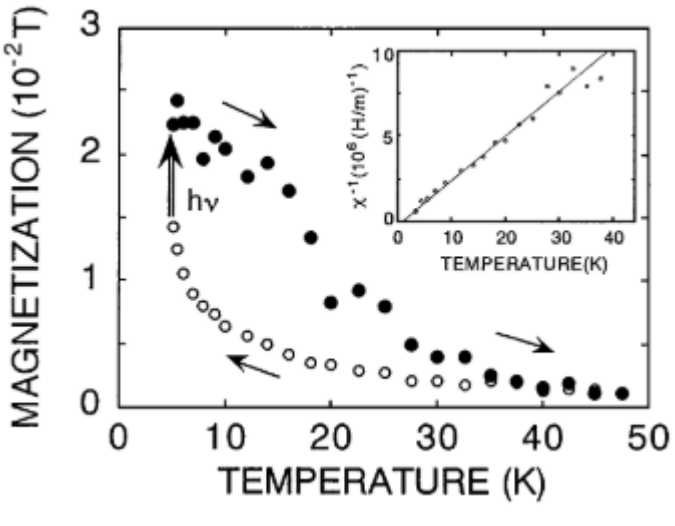

Figure 5: Magnetization vs. Temperature behavior under an illumination procedure described by arrows. The sample is cooled in dark (open circles) to 5 K and then irradiated for 30 min without a magnetic field. It then sits in the dark for 20 min followed by warming up (dark circles) under a magnetic field of 0.02 T. The inset models the Curie-Weiss law for dark start cooling. Image reproduced from[9].

We are excited to test our hypothesis of illumination-controlled magnetism in B-doped CdS. We predict superior results for illumination-controlled magnetism in B-CdS due to CdS's larger and persistent photoconductivity, in comparison to the past work, discussed above.

Literature Review of Boron-doped CdS nanoparticle Synthesis

Synthesis of undoped CdS nanoparticles is well established, with chemical co-precipitation being the popular method. Chemical co-precipitation is the mixing of relevant chemical precursor solutions under defined conditions to precipitate out a desired product. The challenge is to find a chemical co-precipitation synthesis recipe for B-doped CdS nanoparticles. While synthesis of B-doped CdS thin films is well established, synthesis of B-doped CdS nanoparticles is not. We only found one reported synthesis of B-doped CdS nanoparticle synthesis, in literature, by Fakhri et al.[2]. Fakhri et al. used Cadmium Acetate (Cd•Ac) [$Cd(CH_3CO_2)_2 \bullet xH_2O$] as the Cd precursor, Sodium Sulfide [Na_2S] as the sulfur precursor, Boric Acid [H_3BO_3] as the boron precursor, and Polyvinylpyrrolidone (PVP) as a stabilizer, which is used to narrow the size distribution of nanoparticles[2]. For undoped CdS, they dripped 0.5 M Na_2S, aqueous solution, into 0.5 M Cd•Ac, aqueous solution, at 27 °C; then, stirred the resulting solution for 8 h, followed by a Deionized water (DI) and methanol wash, and dried in oven for 6 h at 60 °C[2]. For B-doped CdS, they added 40 mL of 0.25 M H_3BO_3, aqueous solution to the Na_2S solution[2]. Fakhri et al. used X-Ray Diffraction (XRD) to characterize sample composition[2]. Their primary method of characterizing boron doping of CdS nanoparticles was the crystallite size, as calculated via Scherrer's method, band gap energy change, measured via optical spectroscopy, and photoluminescence intensity[2].

SYNTHESIS

Following Fakhri et al.'s recipe, we were able to synthesize undoped CdS nanoparticles but were unable to reproduce their reported success of synthesizing B-doped CdS nanoparticles. We used Inductively Coupled Plasma Optical Emission Spectroscopy (ICP-OES), to characterize boron doping of CdS nanoparticles, which provides the exact sample composition and is a lot more accurate than Fakhri et al.'s characterization approach. We are unsure as to why we were unable to reproduce Fakhri et al.'s work. However, it is possible that the optical change observed by Fakhri et al., attributed to successful boron doping, was actually a result of the change in nanoparticle size. In the absence of other characterization techniques (techniques independent of particle size) to characterize doping, a change in nanoparticle size is not sufficient evidence for doping. Synthesis of undoped CdS nanoparticles is not sufficient validation for Fakhri et al.'s synthesis recipe because a literature survey of undoped CdS synthesis reveals that undoped CdS synthesizes very readily as long as there is a Cd and a S precursor[10]–[17].

We decided to develop our own recipe for B-doped CdS nanoparticles by reviewing the synthesis of other doped-CdS nanoparticle systems.

Precursor Choice

A chemical co-precipitation synthesis recipe is largely defined by the precursors it uses. It factors such as concentration, stabilizer choice, and temperature, also play a role but they work around the precursor choice. Cd•Ac and Na_2S precursors were retained because of their popularity with doped-CdS systems[18]–[21], and H_3BO_3 was also retained because we did not find an alternative boron precursor. We did not observe a significant change in nanoparticle size distribution due to PVP addition, so we decided not to use it. Also, nanoparticle size distribution

is not a relevant variable for our experiment, as our characterization techniques report bulk properties. We also observed that other reports of doped-CdS systems used much lower precursor concentrations than Fakhri et al., 0.5 M[18]–[21]. During doping of CdS, the goal is to have the dopant incorporated into the CdS nanoparticle during the formation of the nanoparticle. This can be difficult to achieve because, kinetically, CdS formation is greatly favored and the CdS nanoparticles form very rapidly, leaving very little time for the dopant to be incorporated into them. The rapid formation of CdS is easily observed in synthesis, where the color of the cadmium precursor rapidly changes to orange upon the smallest addition of the sulfur precursor. To increase the chances of successful boron doping of CdS, we decided to use a low cadmium/sulfur precursor concentration and a high boron precursor concentration. We used a 0.75 M concentration for the boron precursor, which was very close to the maximum solubility of Boric Acid in water. We used a 0.1 M concentration for the cadmium/sulfur precursors, which was the lowest concentration that yielded a reasonable sample volume. By increasing the boron precursor concentration and lowering the cadmium/sulfur precursor concentration, we slow down CdS formation while speeding up boron inclusion.

Determining the right configuration for adding the boron precursor

There are two ways to add the boron precursor to the CdS system. One way is to have the boron present during the CdS formation, and the other way is to add the boron during the CdS formation. We conducted a limited study of both of these methods.

CdS formation in the presence of boron

25 mL of 0.1 M Cd•Ac were dripped (at a rate of 1 drop/sec) into a 250 mL beaker containing 25 mL of 0.1 M Na_2S and **"*x*"** mL of **"*y*"** M H_3BO_3. A water bath was used to

maintain the temperature at 30 °C. The solution was vigorously stirred, with a magnetic stirrer, during the addition of the Cd•Ac solution. Then the final mixture was stirred for 2 hrs. The solution was then washed, dried, and made into fine powder. There were several samples made with varying precursor volume and concentration:

i. Undoped CdS
   - no H_3BO_3 was used

ii. Control boron doping
   - 25 mL of 0.75 M H_3BO_3

iii. Concentration study with varying H_3BO_3 concentration and constant H_3BO_3 volume
   - 25 mL of 0.6 M H_3BO_3
   - 25 mL of 0.45 M H_3BO_3

iv. Volume study with varying H_3BO_3 volume and constant H_3BO_3 concentration
   - 20 mL of 0.75 M H_3BO_3
   - 15 mL of 0.75 M H_3BO_3

CdS formation with boron addition

25 ml of 0.1 M Na_2S and ***"x"*** mL of ***"y"*** M H_3BO_3 were dripped (at a rate of 1 drop/sec) into a 250 mL beaker containing 25 mL of 0.1 M Cd•Ac. A water bath was used to maintain the temperature at 30 °C. The same after procedure was followed above. The solution was vigorously stirred, with a magnetic stirrer, during the addition of the Na_2S/H_3BO_3 solution. Then the final mixture was stirred for 2 hrs. The solution was then washed, dried, and made into fine powder. A temperature study was performed after encouraging initial results. The concentration and volume studies were interrupted.

i. Undoped CdS
   - no H_3BO_3 was used

ii. Control boron doping
   - 25 mL of 0.75 M H_3BO_3

iii. Concentration and volume study interrupted by the Covid-19 pandemic

iv. Temperature study
   - 25 mL of 0.75 M H_3BO_3 at 35 °C
   - 25 mL of 0.75 M H_3BO_3 at 40 °C
   - 25 mL of 0.75 M H_3BO_3 at 45 °C

Cobalt-doped Cadmium Sulfide nanoparticles

Cobalt-doped CdS nanoparticles were also made as a comparison with a traditional magnetic dopant, as in literature[22]. Cobalt(II) Acetate Tetrahydrate (Co•Ac) [$Co(CH_3CO_2)$ $•4H_2O$] was used as the cobalt precursor; Cd•Ac and Na_2S used as cadmium and sulfur precursors, respectively. 20 mL of 0.2 M Na_2S were dripped into a 250 mL beaker containing 20 mL of 0.2 M Cd•Ac and 1 mL of 0.2 M Co•Ac, at room temperature. The solution was vigorously stirred, with a magnetic stirrer, during the addition of the Na_2S solution. Then the final mixture was stirred for 4 hrs. The solution was then washed, dried, and made into fine powder.

Washing and Drying Procedure

After stirring for 2 hrs, the precipitate was allowed to accumulate at the bottom of the beaker and the excess liquid on top was decanted. The remaining solution was then washed,

three times, with DI water of three times the volume of the solution. Followed by a wash, three times, with methanol of two times the volume of the solution. The remaining solution was heated on a hotplate at 70 °C. The precipitate was considered sufficiently dried, when dark-orange pieces were left at the bottom of the beaker. The dried precipitate was crushed into a fine powder with a mortar-pestle and stored in a glass vial.

Observations

- We used a stirring time of 2 hrs as opposed to the 8 hrs in literature[2], because we did not observe a significant difference in boron doping between 2 hrs and 8 hrs.
- Successfully b-doped CdS samples were yellower than undoped CdS samples and appeared less dense.
- An exact heating time should not be used because the volume of the remaining liquid after washing varies, which affects evaporation and thereby total drying time. Instead, sample dryness should be judged by precipitate behavior, as described above.
- It was also observed that successfully doped samples featured a unique color transition during the precursor combination. Instead of becoming orange right away, they maintained a light-yellow intermediate phase. For optimal doping, the light-yellow phase should be maintained by controlling the dripping rate and the stirring rate. The dripping rate should be slow enough that CdS formation is not too quick, which is observed by a rapid, irreversible orange color, and the stirring rate should be fast enough to quickly disperse the drops in the whole solution so CdS is not rapidly formed in a local region. By balancing the two levers, a light-yellow phase can be maintained. We believe that the light-yellow phase is associated

with successful doping because it features a slower CdS formation which provides enough time for boron to be incorporated.

CHARACTERIZATION

Powder X-Ray Diffraction (XRD)

PANalytical X'Pert Pro multipurpose diffractometer was used to perform powder XRD on bulk powder samples for insight into the structural and phase composition. The standard powder packing procedure was followed to prepare the powder samples for XRD measurements. Analysis was performed via the High Score Plus software.

Inductively Coupled Plasma Optical Emission Spectroscopy (ICP-OES)

ICP-OES was used to measure the chemical composition of the powder samples via the Agilent ICP-OES VDV 5100 spectrometer. The measurements were taken in the radial view. The 249.678 nm, 508.525 nm, and 228.615 nm wavelengths were used to measure the boron, cadmium, and cobalt concentrations, respectively.

Standard preparation: Single element standards were purchased from Inorganic Ventures. All standards had a 2% HNO_3 matrix. For boron, calibration standards of 10, 20, and 30 µg/mL concentrations were prepared by diluting a 1,000 µg/mL standard by 2% HNO_3. For cadmium, calibration standards of 500, 750, and 1000 µg/mL concentrations were prepared by diluting a 10,000 µg/mL standard by 2% HNO_3. For cobalt, calibration standards of 10, 50, and 100 µg/mL concentrations were prepared by diluting a 10,000 µg/mL standard by 2% HNO_3. All calibration standards were filtered by a 0.2 µm filter and transferred to a 15 mL centrifuge tube.

Sample Preparation: 40 mg of sample powder was dissolved in 1 mL of 68% Nitric Acid (HNO_3) and heated on a hotplate at 70 °C until the solution was clear. Then the sample solution

was diluted to 2% HNO_3. 5 mL of the sample solution were filtered by a 0.2 μm filter and transferred to a 15 mL centrifuge tube.

Analysis: Element concentrations were converted to μg/mL from ppm and then normalized to moles to determine their respective molar ratios. A conversion factor of 1 ppm = 1 μg/mL was used to convert between the two units. However, the proper conversion factor is 1 ppm = 1 μg/g, which requires normalization with respect to solution densities. Due to the covid-19 disruption, we could not obtain the solution densities and instead used the 1 ppm = 1 μg/mL, which is a sufficient approximation.

Magnetometry

DC Magnetic measurements were taken via a Quantum Design MPMS3 Superconducting Quantum Interference device (SQUID). Magnetization vs. Temperature curves were taken from 300 K to 2 K, at 10,000 Oe. Magnetization vs. Magnetic Field curves were taken from -10,000 Oe to +10,000 Oe, at specific temperatures.

Sample Preparation: Powder samples were tightly packed in a plastic capsule. A straw holder was used to hold the capsule.

$$\boldsymbol{\chi = \frac{M}{H} = \frac{N \cdot \mu^2}{3 \cdot A \cdot k \cdot (T - T_C)} + \chi_{diamagetic}}$$

Equation 1: Curie-Weiss Law

Analysis: Mathematica was used to fit the Curie-Weiss law, equation 1, to the magnetization vs. temperature data. In equation 1, χ is the mass susceptibility, M is magnetization, H is magnetic field, N is Avogadro's number, μ is the magnetic moment per formula unit, A is atomic mass, k

is Boltzmann's constant, T is temperature, T_C is the curie temperature, and $\chi_{diamagnetic}$ is the diamagnetic susceptibility that is inherent to all materials. A 95% confidence interval was calculated to estimate error in magnetic data.

RESULTS

Undoped-CdS nanoparticles

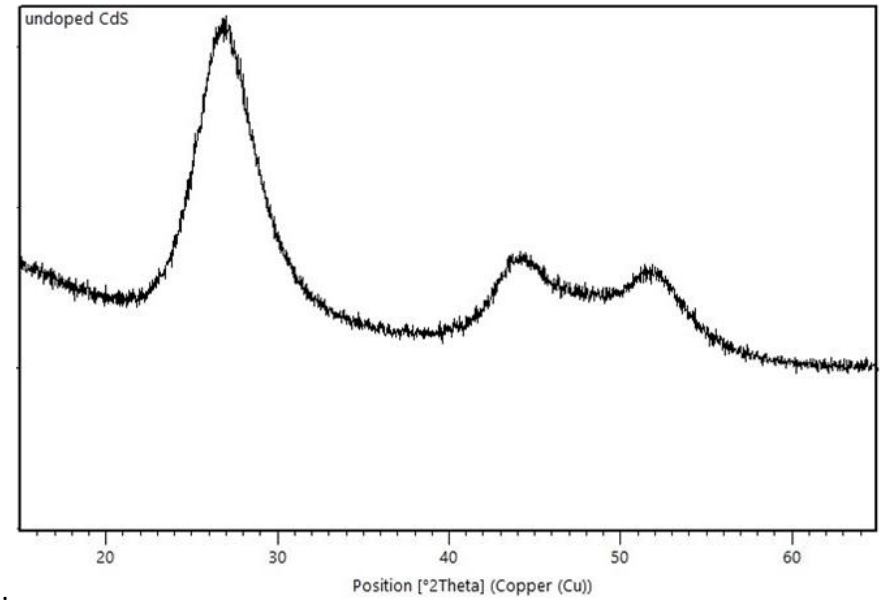

Figure 6: XRD Spectra of undoped-CdS with 2Θ peaks: 26.87 (111), 29.00 (002), 43.82 (200), 52.00 (113).

The XRD spectra of our undoped-CdS in Figure 6, agrees well with the cubic CdS phase of reference pattern (96-101-1261). Despite the cubic crystallinity of our undoped-CdS sample, we still observe a broadening of the peaks. We believe that the small 2-5 nm size, as calculated via Scherrer's formula, of our nanoparticles is approaching the diffractometer's resolution limit, in which the small nanoparticle size has an effect, on the XRD spectra, similar to amorphous materials. Figure 7 shows the magnetometry data for the undoped-CdS. As expected, the undoped-CdS exhibits diamagnetic behavior and our measured diamagnetic susceptibility, calculated from Curie-Weiss, of $3.34*10^{-7}$ emu/g agrees really well with reference value in literature[21][23]. In Figure 7a, small paramagnetic behavior is observed at lower temperature; however, it is negligible and is most likely due to contamination during synthesis or handling. In

Figure 7b, we observe strong diamagnetism at higher temperatures and an insignificant drop in the diamagnetism at lower temperatures, which agrees with the behavior, in Figure 7a, for insignificant paramagnetic trace contaminants. A magnetic moment of 0.029 bohr magnetons,

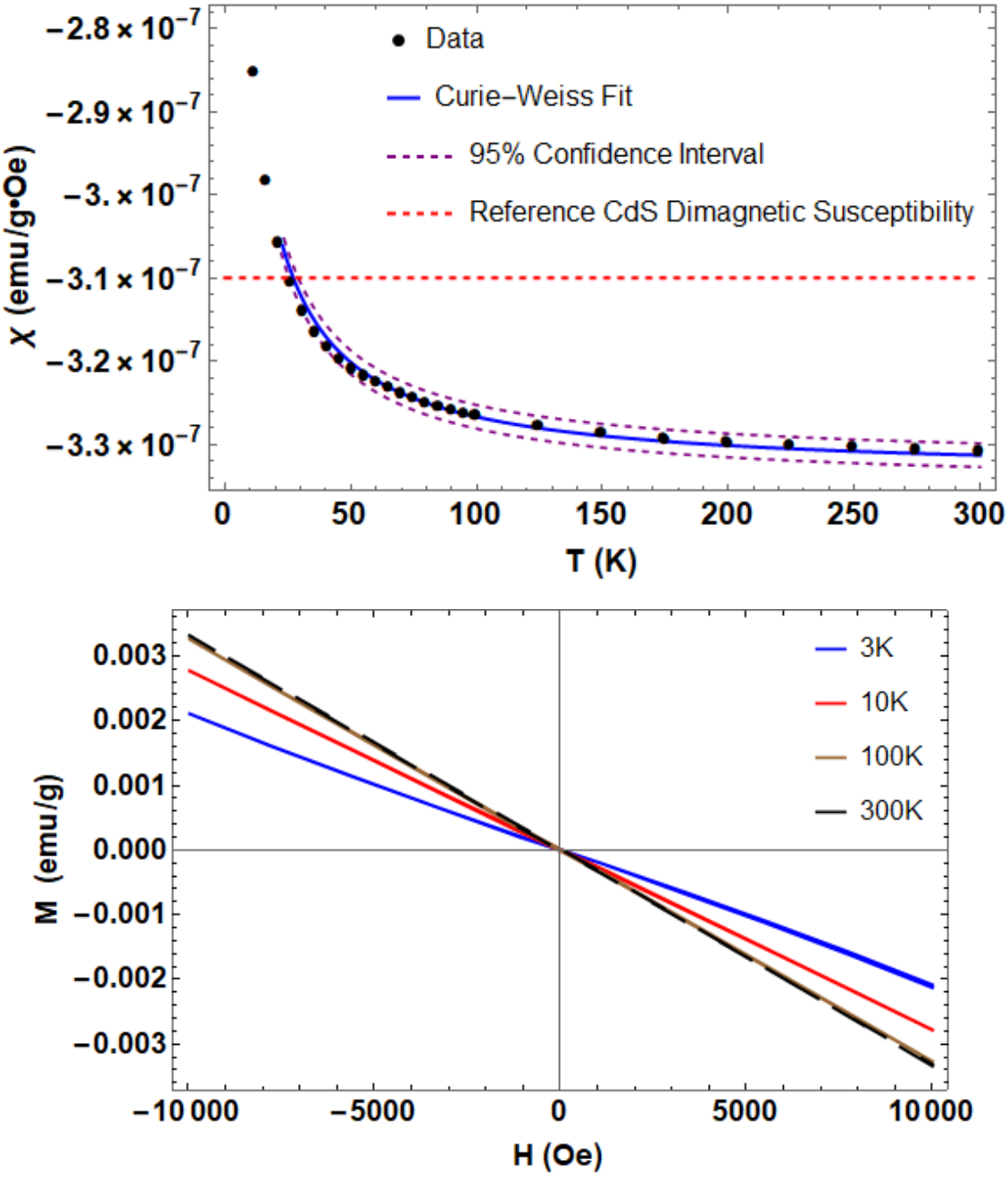

Figure 7. Magnetometry data for undoped CdS (a) χ vs. T (b) M vs. H

normalized by formula unit, was measured which was attributed to the trace contaminants.

CdS nanoparticles formed in presence of the boron precursor

Control boron doping

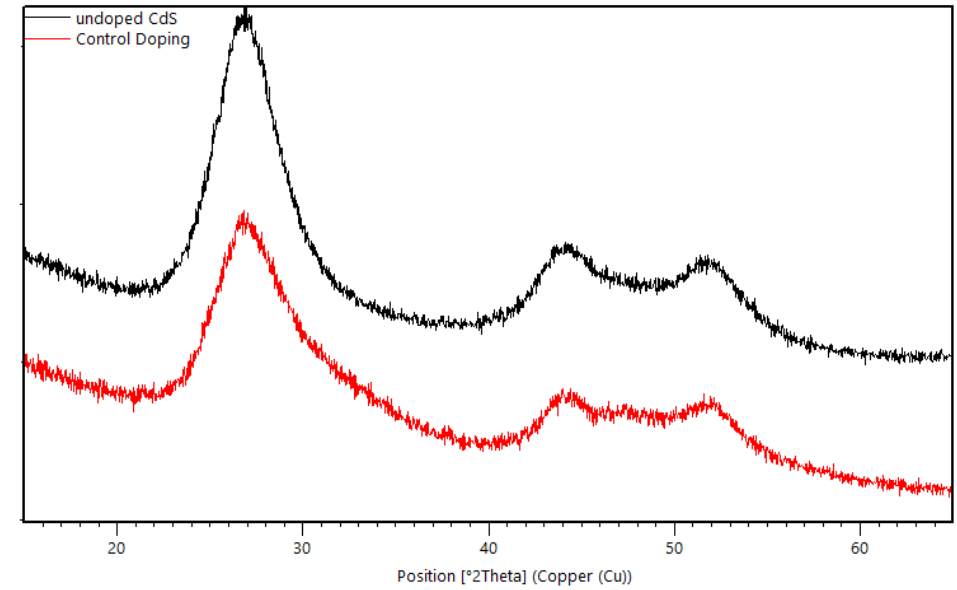

.

Figure 8: XRD Spectra of control boron (25mL 0.75M H_3BO_3 with H_3BO_3 present) doping with 2Θ peaks: 26.84 (111), 30.0 (002), 44.63 (200), 51.11 (113).

Figure 8 shows the XRD for the control boron doping condition, where the control-doping spectra is characteristic of the cubic CdS phase, just like undoped CdS. ICP-OES analysis found the control doping boron sample to have a B:Cd ratio of 0.62. It was surprising that this high molar ratio was not represented in the XRD spectra as a consistent peak-shift or peak-broadening. While some peaks did shift a little, the shift was not consistent as the most significant 111 beak did not shift towards larger 2Θ.

Volume study of boron doping

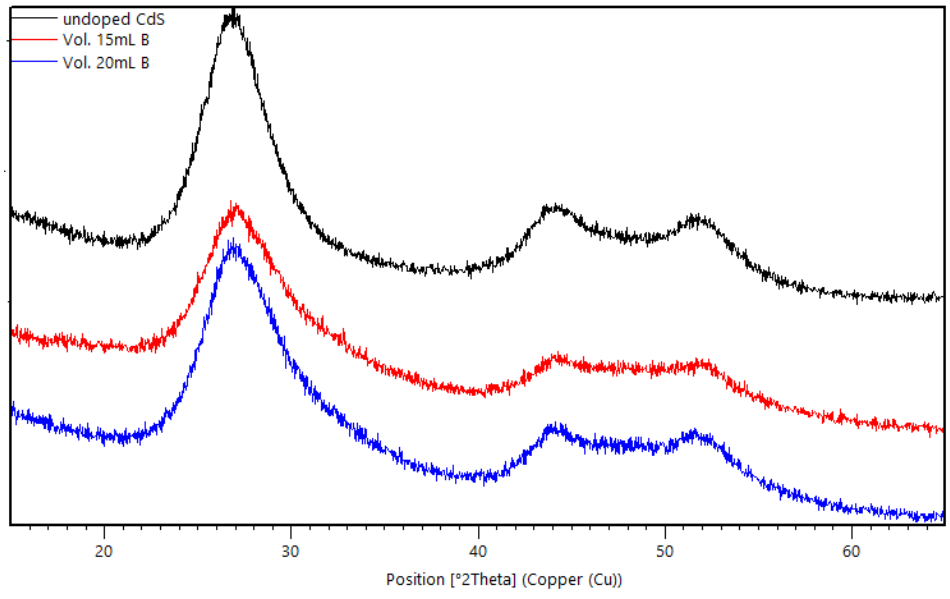

Figure 9: XRD Spectra of the volume study of boron doping with 2Θ peaks: [red] 15 mL H_3BO_3: 26.95 (111), 30.00 (002), 44.63 (200), 51.00 (113) [blue] 20mL H_3BO_3: 26.93 (111), 30.00 (002), 44.36 (200), 51.08 (113).

Figure 9 shows the XRD spectra for the volume study of boron doping samples, where 15 mL and 20 mL of 0.75 M H_3BO_3 were used instead of 25 mL. The 15 mL H_3BO_3 and 20 mL H_3BO_3 were measured to have a B:CdS ratio of 0.38 and 0.37, respectively. This was reflected in the XRD spectra with a consistent peak-shift throughout spectra, with the significant 111 peak-shifting by 0.08 (15 mL) and 0.06 (20 mL) 2Θ.

Concentration study of boron doping

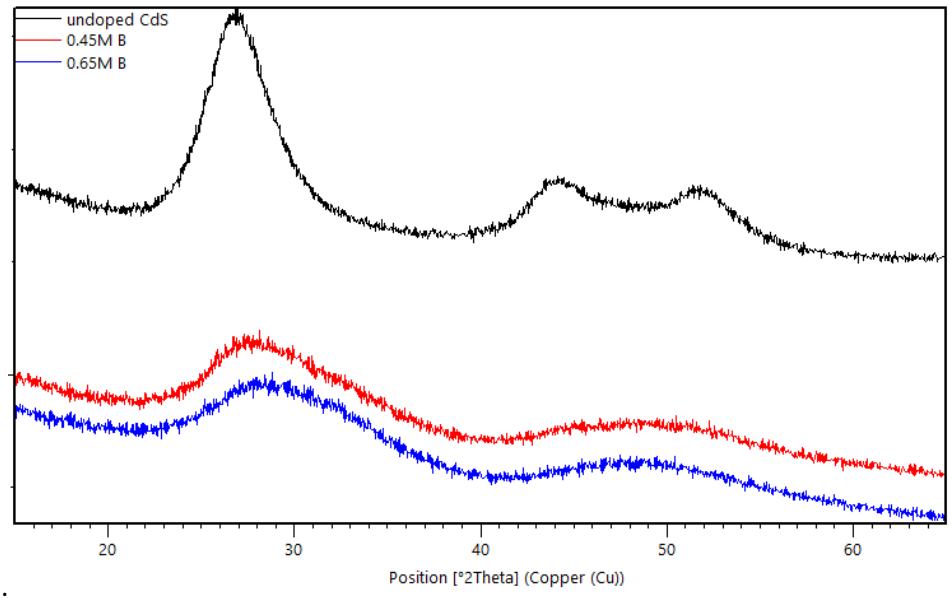

Figure 10: XRD Spectra of the concentration study of boron doping with 2Θ peaks: [red] 0.45 M H_3BO_3: 27.5 (111), 32.10 (002), 45.40 (200), 50.5 (113) [blue] 0.60 M H_3BO_3: 28.00 (111), 33.00 (002), 47.50 (200), 52.00 (113).

Figure 10 shows the XRD spectra for the concentration study of boron doping samples, where 25 mL of 0.45 M and 0.60 M of H_3BO_3 were used instead of 0.75 M. The 0.45 M H_3BO_3 and 0.60 M H_3BO_3 were measured to have a B:CdS ratio of 0.84 and 1.11, respectively. This was reflected in the XRD spectra with a consistent peak-shift throughout spectra, with the significant 111 peak shifting by 0.63 (0.45 M) and 1.13 (0.60 M) 2Θ. However, these molar ratios are extremely high and indicate boron inclusion in a secondary phase in addition to doping. Figure 11 shows the magnetometry data for the 0.60 M H_3BO_3 sample. Despite the high boron concentration, measured quantitatively via ICP-OES and qualitatively via XRD peak shift, no significant magnetic behavior was detected. A magnetic moment of 0.038 bohr magnetons, normalized by formula unit, was detected which was consisted with what would be expected

from trace contaminants. The diamagnetic behavior observed in Figure 11a and 11b are consistent with that we observed in undoped CdS in Figure 7.

Magnetometry data for other samples was disrupted due to Covid-19.

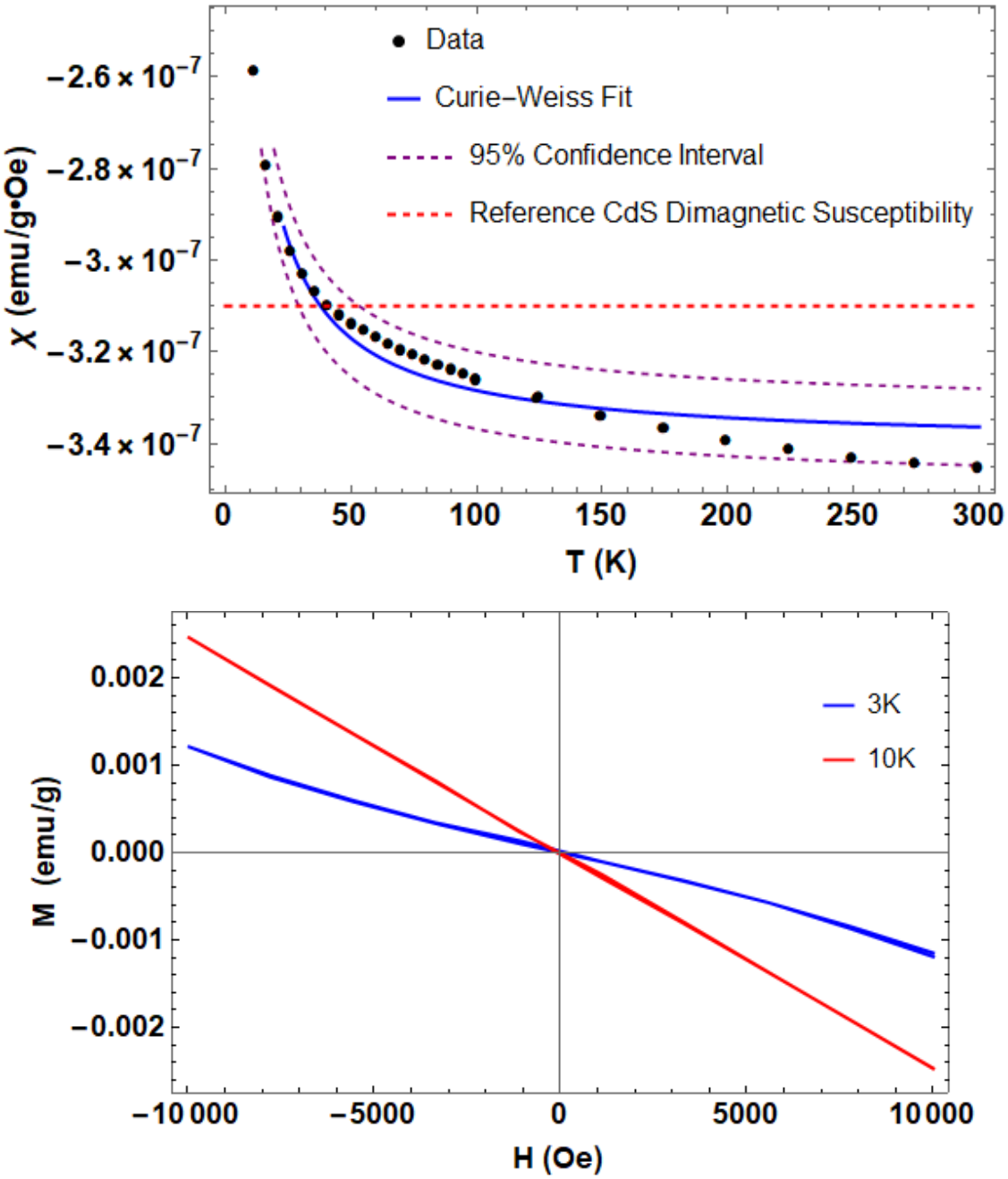

Figure 11: Magnetometry data for 0.60 M H_3BO_3 (a) χ vs. T (b) M vs. H

CdS nanoparticles formed with addition of the boron precursor

Control Doping

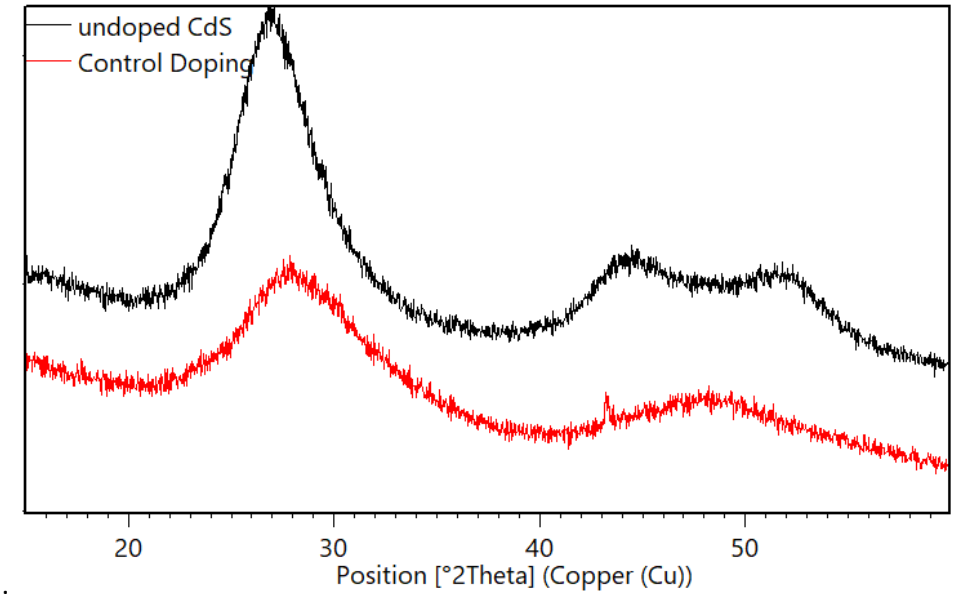

Figure 12: XRD Spectra of control doping (25mL 0.75M H_3BO_3 with H_3BO_3 added) with 2Θ peaks: 27.80 (111), 33.00 (002), 43.22 (200), 47.86 (113).

Figure 12 shows the XRD spectra of the control doping which shows significant peak-shifting and broadening, indicative of successful doping. B:Cd ratio was measured to be 0.58 via ICP-OES. The 111 peak shifted by 0.93 toward higher 2Θ which indicates boron inclusion within the lattice. The broadening of the peaks is likely due to the deterioration of crystalline order due to dopant inclusion in the lattice. It is interesting to note that the higher 2Θ peaks merge into a broader peak. Significant paramagnetic behavior was observed, as seen in Figure 13. In Figure 13a and 13b, paramagnetic behavior emerges with decreasing temperature and in Figure 13b explicit paramagnetic behavior is seen at 3K. We calculated a magnetic moment of 0.54 bohr magnetons per boron atom, which is in the same order of magnetic as Bedolla et al.

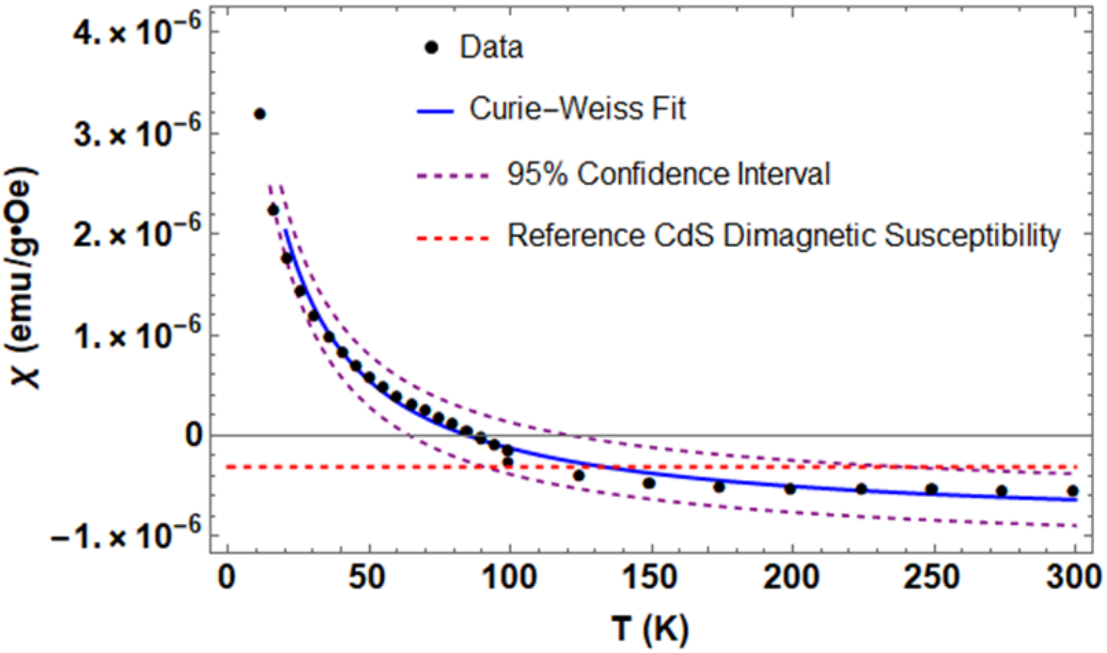

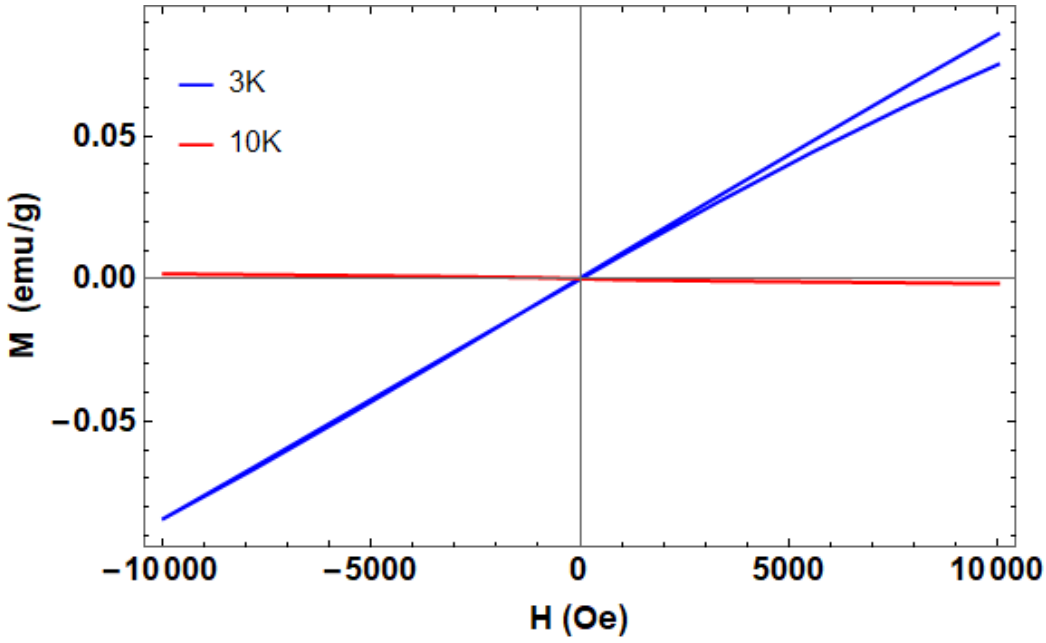

Figure 13: Magnetometry data for control doping (a) χ vs. T (b) M vs. H

Temperature study of CdS nanoparticles with boron addition of the boron precursor

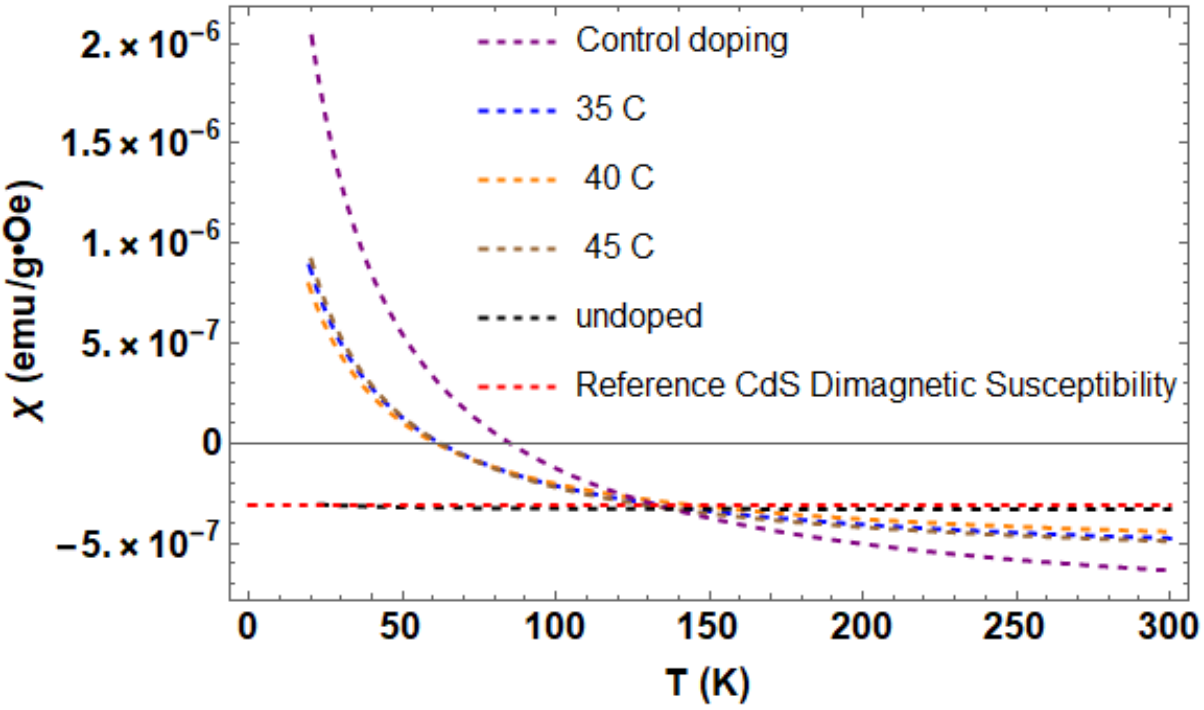

Figure 14. Magnetic Summary of Temperature study with Curie-Weiss fit for each sample.

Figure 14 is the magnetic summary of the temperture study, with Curie-Weiss fits, with doped CdS formed with boron addition. The CdS samples formed with boron precursor addition have shown significant paramgnetic behavior. The 35 °C, 40 °C, and 45 °C samples were measured to have B:Cd ratios of 0.38, 0.59, and 0.78, respectively. With boron inclusion increasing with temperature. However, the three temperatures observed the same paramagnetic profile despite varrying boron concentration, which indicates magnetic saturation at a lower B:Cd ratio. The calculated magnetic moments per bohr magneton for 35 °C, 40 °C, and 45 °C was 0.597, 0.371, and 0.295, respectively. Which is expected to decrease with increasing temperature, because the magnetic signal is saturated while B:Cd ratio increases. It should be noted that the diamagnetic behavior of the undoped CdS sample agrees really well with reference

data. Also, the control doing sample has a stronger paramagnetic response which needs to be further investigates. Future samples will be made at a 45 °C with lower boron precursor concentrations to find the B:Cd ratio with the saturated magnetic behavior. Figures 15, 16, and 17, show the detailed magnetometry data for 35 °C, 40 °C, and 45 °C, respectively. The magnetization vs. magnetic field curves show a diverge at lower temperatures, which we hypothesize is due to friction of the straw with the inner wall, caused by the straw's rigidity at lower temperatures. We can use a quartz holder in the future, to eliminate this.

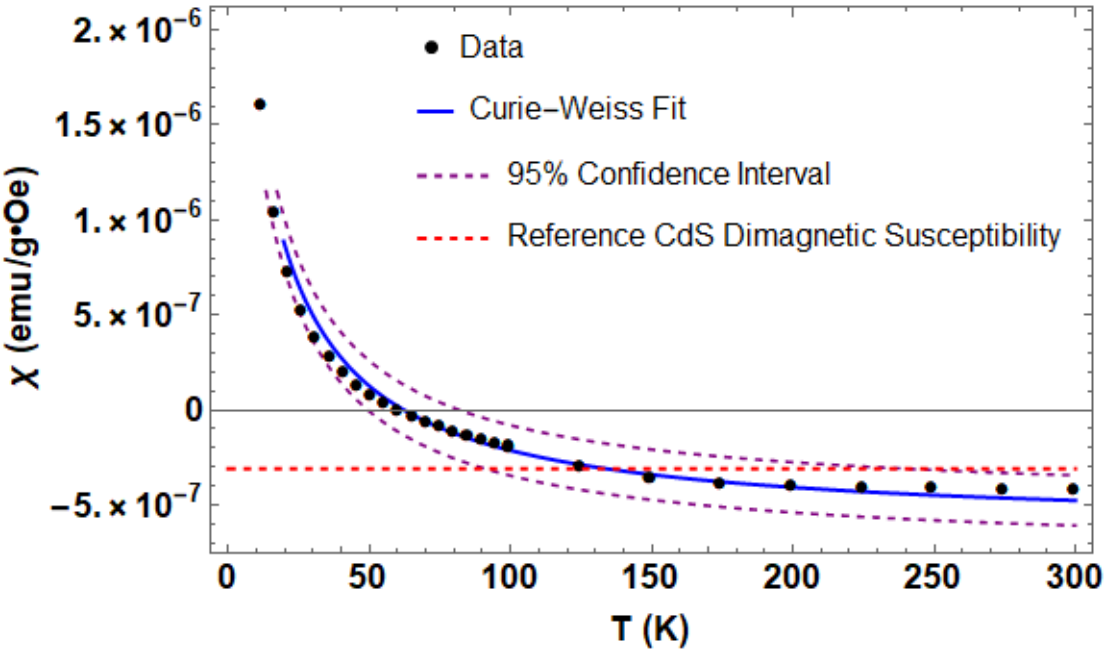

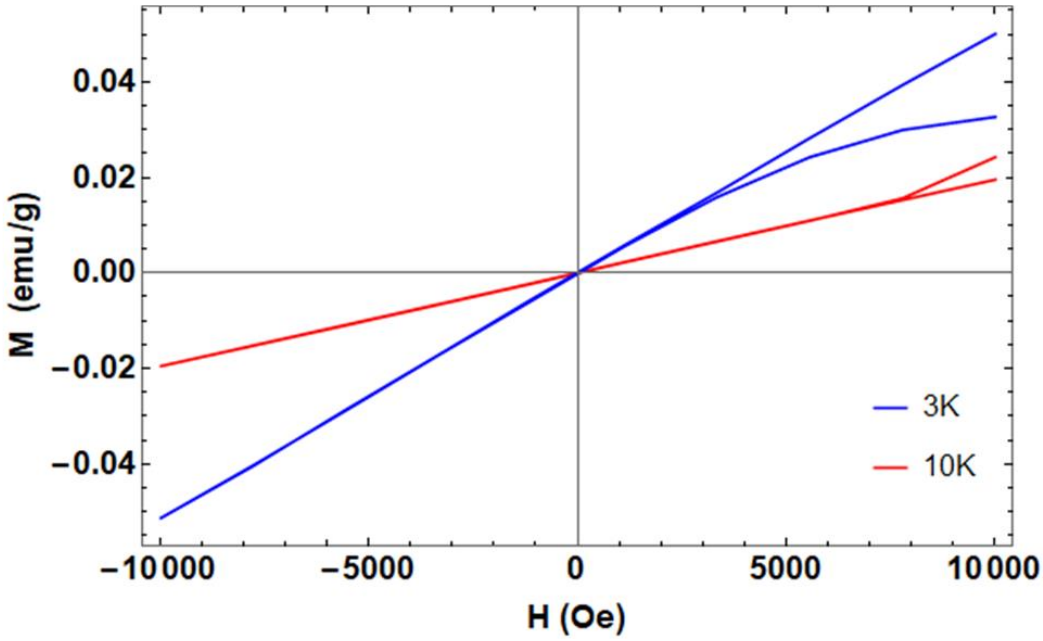

Figure 15: Magnetometry data for 35 °C (a) χ vs. T (b) M vs. H

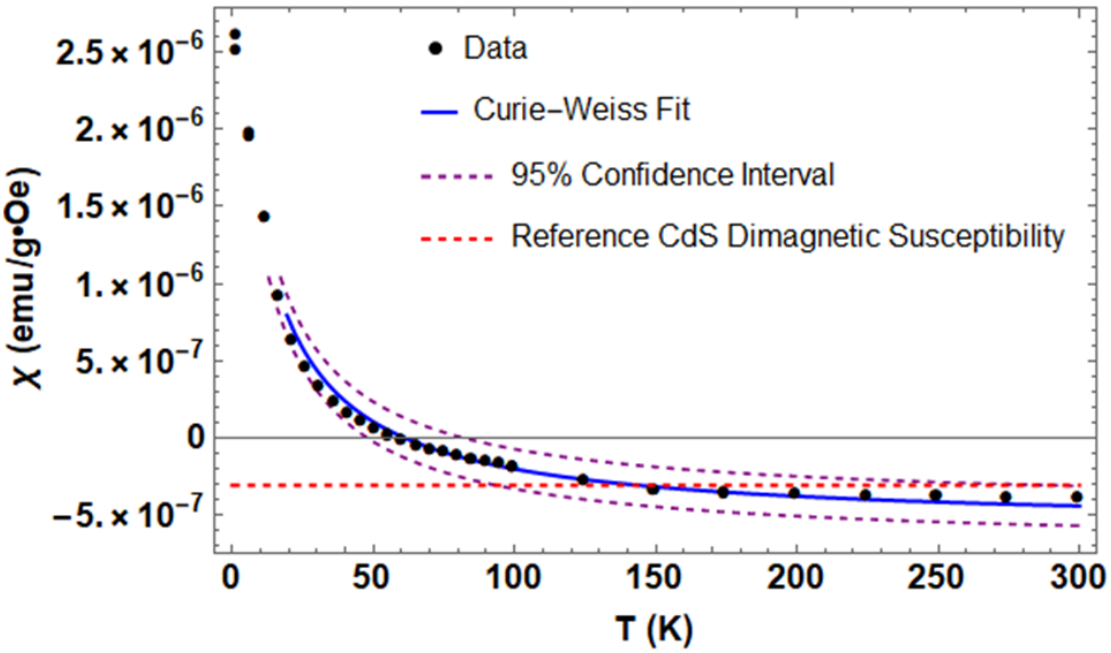

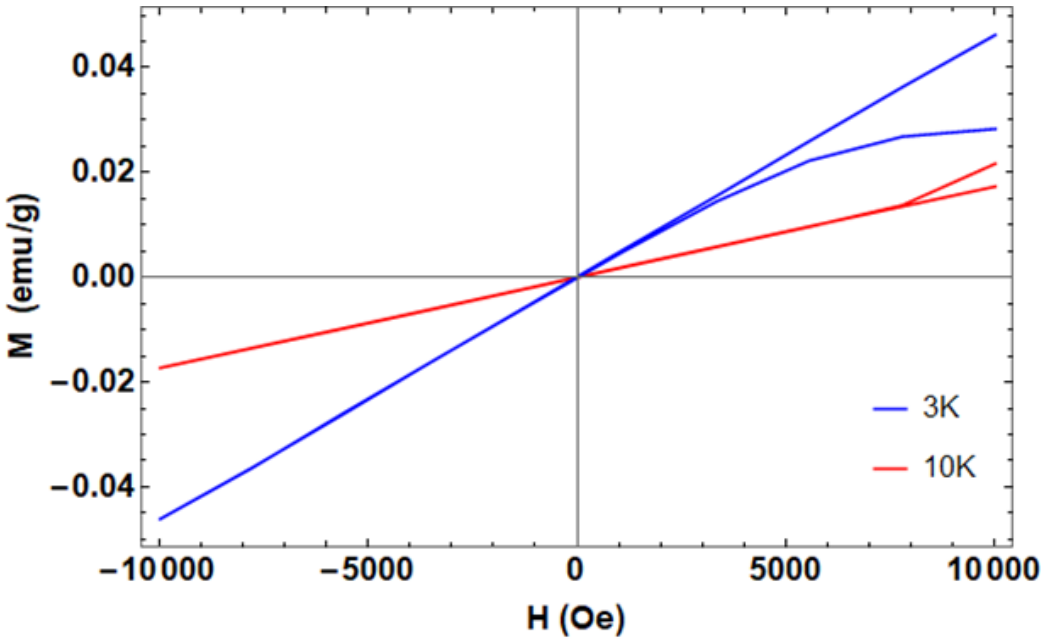

Figure 16: Magnetometry data for 40 °C (a) χ vs. T (b) M vs. H

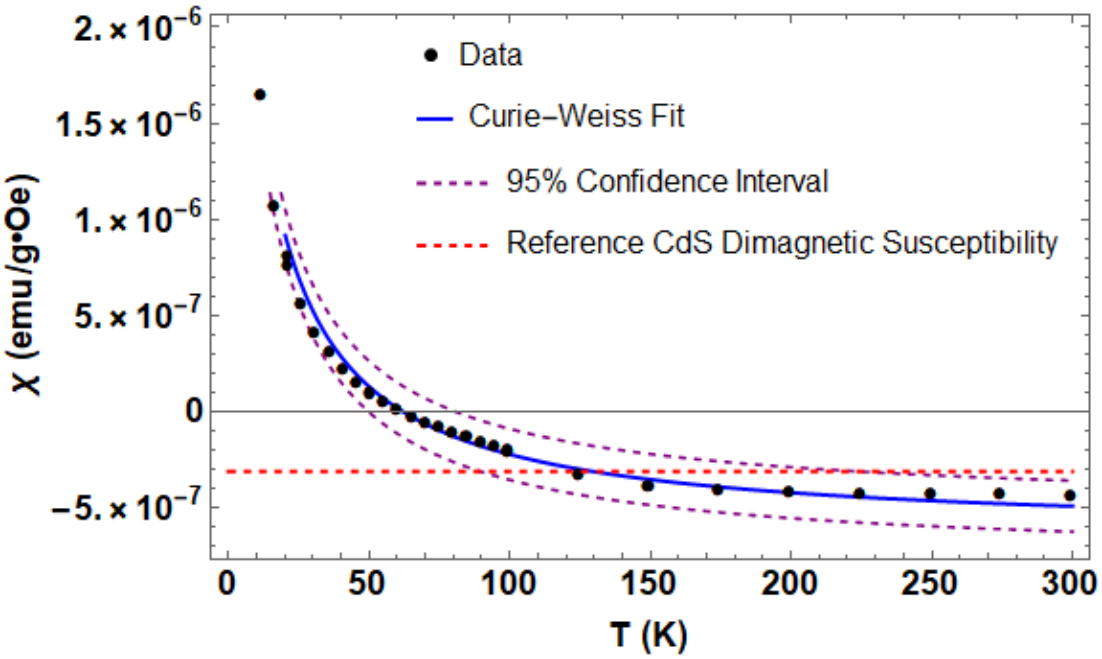

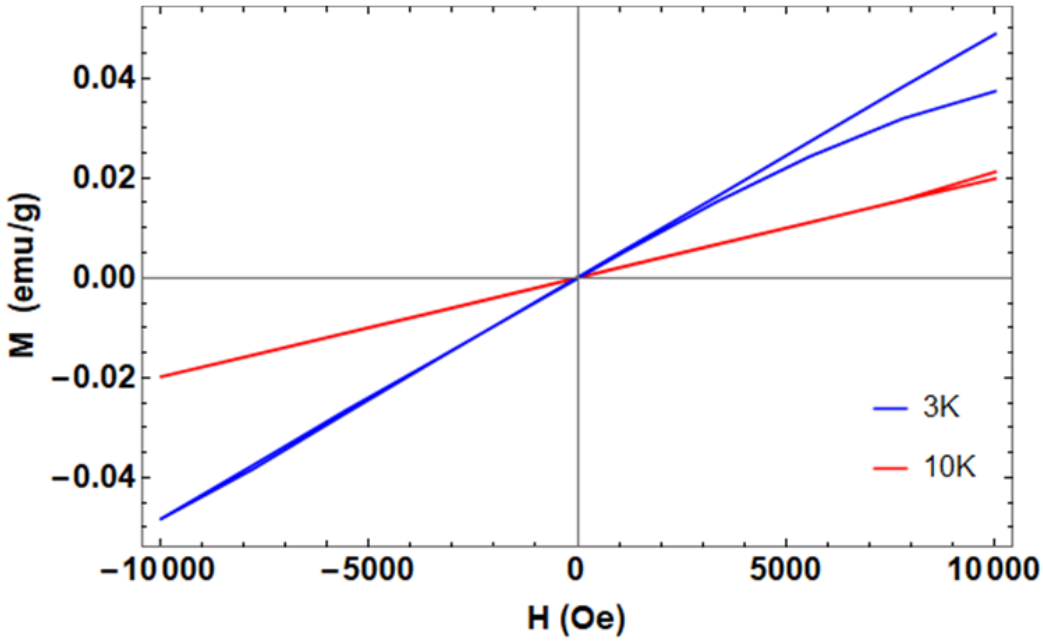

Figure 17: Magnetometry data for 45 °C (a) χ vs. T (b) M vs. H

Cobalt-doped CdS nanoparticles

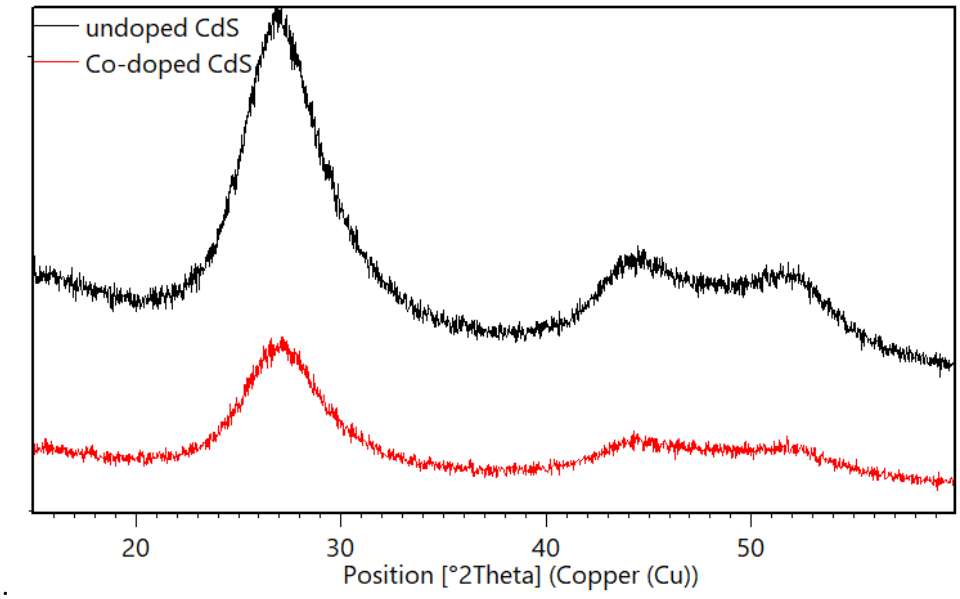

Figure 18: XRD Spectra of Cobalt doped CdS 2Θ peaks: 26.95 (111), 30.00 (002), 44.58 (200), 51.11 (113).

Figure 18 shows the XRD spectra of Co-doped CdS nanoparticles. The XRD for Co-doped CdS spectra agrees with the cubic CdS phase. ICP-OES measured a Co:CdS ratio of 0.02. There is peak-shifting and broadening which is consistent for doping. Figure 19 shows the magnetometry data for Co-doped CdS which exhibits strong paramagnetic behavior, as in literature[24].

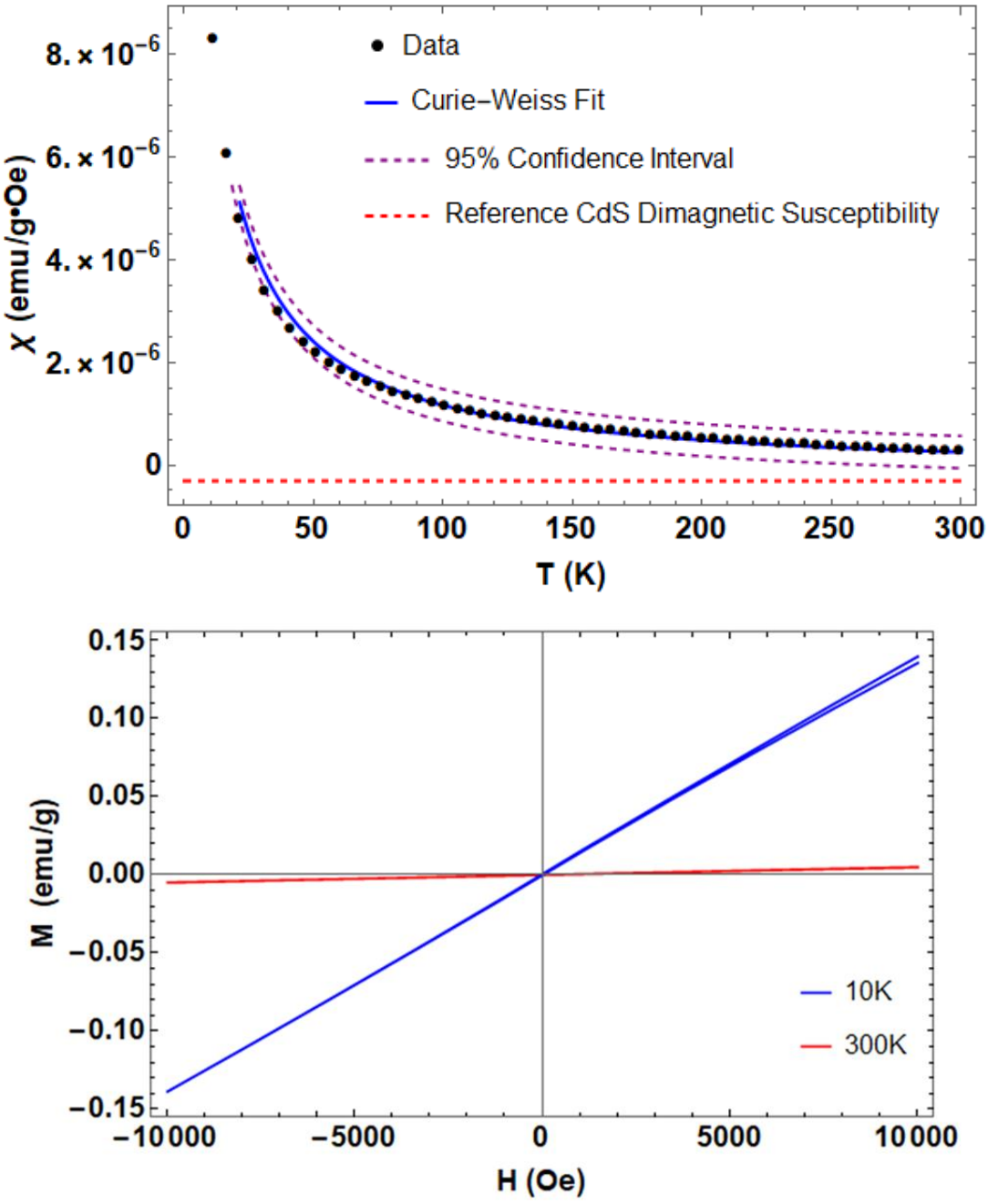

Figure 19. Magnetometry data for Cobalt-doped CdS (a) χ vs. T (b) M vs. H

CONCLUSION

We have successfully confirmed the theoretical prediction of emergent magnetism from non-magnetic Cd and B. Our next steps are to conduct an illumination-magnetism study by taking magnetic measurements under illumination, to see if we can use illumination to control the magnetic behavior. Also, our dopant to Cd ratio were very high and will be investigated. We will use EDX and SEM to further understand the chemical composition to identify the reason for high dopant concentrations measured via ICP-OES. A concentration and volume study will be performed with CdS nanoparticles formed with boron addition, to lower the B:Cd ratio and identify the B:Cd ratio corresponding to magnetic saturation.

SAMPLE DESCRIPTION

Sample ID	**Sample description**	**T_c [± 5.0]**	**μ/F.U [± 0.04]**	**Figures**
0125_CdS_2	undoped CdS	-3.4	0.029	6, 7
0125_CdBS_1	25mL of 0.75M H_3BO_3 present [Control doping]	N/A	N/A	8
0126_CdBS_15mL_1	15mL of 0.75M H_3BO_3 present	N/A	N/A	9
0126_CdBS_20mL_1	20mL of 0.75M H_3BO_3 present	N/A	N/A	9
0127_CdBS_15mL	25mL of 0.45M H_3BO_3 present	N/A	N/A	10
0127_CdBS_20mL	25mL of 0.60M H_3BO_3 present	-2.6	0.038	10, 11
1019_30C_hBS	25mL of 0.75M H_3BO_3 added [Control doping]	-8.6	0.54	12, 13
0216_35C_hBS	25mL of 0.75M H_3BO_3 added @ 35C	-10	0.597	15
0216_40C_hBS	25mL of 0.75M H_3BO_3 added @ 40C	-11	0.371	16
0216_45C_hBS	25mL of 0.75M H_3BO_3 added @ 45C	-8.9	0.295	17
0721_CdS_Co#	Described in Synthesis section	-6.4	20.57	18, 19

Table 1: Sample ID is the sample name found in lab notebook. Sample description describes the synthesis. Present means that H_3BO_3 was present during CdS synthesis and added means that H_3BO_3 was added during CdS synthesis. N/A means that magnetic data is unavailable. T_c is the Curie Temperature with an error of ± 5.0, estimated from variation of samples with the same B:Cd ratio. μ/F.U is the magnetic moment in bohr magnetons per CdS formula unit (F.U) for undoped sample or per bohr atom for doped samples; the error is ± 0.04 estimated from variation due to contaminants. Figures lists the relevant figures for each sample.

ACKNOWLEDGEMENTS

I would like to thank Professor Rafael Jaramillo without whose mentorship, this thesis would not have been possible. I want to acknowledge Dr. Charlie Settens for his valuable insight in XRD analysis and Ulugbek Barotov for his critical assistance with designing the synthesis experiments. While NMR spectroscopy was eventually not pursed, I want to acknowledge Walter Massefski for his dedicated help with NMR measurements and analysis, at the beginning of our experiment.

REFERENCES

[1] P. O. Bedolla, C. Gruber, P. Mohn, and J. Redinger, "p-electron magnetism in CdS doped with main group elements," *J. Phys. Condens. Matter*, vol. 24, no. 47, p. 476002, Nov. 2012.

[2] A. Fakhri and R. Khakpour, "Synthesis and characterization of carbon or/and boron-doped CdS nanoparticles and investigation of optical and photoluminescence properties," *J. Lumin.*, vol. 160, pp. 233–237, Apr. 2015.

[3] T. Dietl, "Functional ferromagnets," *Nat. Mater.*, vol. 2, no. 10, pp. 646–648, Oct. 2003.

[4] H. Pan, Y. P. Feng, Q. Y. Wu, Z. G. Huang, and J. Lin, "Magnetic properties of carbon doped CdS: A first-principles and Monte Carlo study," *Phys. Rev. B*, vol. 77, no. 12, p. 125211, Mar. 2008.

[5] H. Yin, A. Akey, and R. Jaramillo, "Large and persistent photoconductivity due to hole-hole correlation in CdS," *Phys. Rev. Mater.*, vol. 2, no. 8, p. 084602, Aug. 2018.

[6] T. Dietl and H. Ohno, "Dilute ferromagnetic semiconductors: Physics and spintronic structures," *Rev. Mod. Phys.*, vol. 86, 2014.

[7] T. Dietl, "Zener Model Description of Ferromagnetism in Zinc-Blende Magnetic Semiconductors," *Science (80-.).*, vol. 287, no. 5455, pp. 1019–1022, Feb. 2000.

[8] J. Wang, I. Cotoros, K. M. Dani, X. Liu, J. K. Furdyna, and D. S. Chemla, "Ultrafast Enhancement of Ferromagnetism via Photoexcited Holes in GaMnAs," *Phys. Rev. Lett.*, vol. 98, no. 21, p. 217401, May 2007.

[9] S. Koshihara *et al.*, "Ferromagnetic Order Induced by Photogenerated Carriers in Magnetic III-V Semiconductor Heterostructures of (In,Mn)As/GaSb," *Phys. Rev. Lett.*, vol. 78, no. 24, pp. 4617–4620, Jun. 1997.

[10] R. Bhattacharya and S. Saha, "Growth of CdS nanoparticles by chemical method and its characterization," 2008.

[11] P. Chandran, P. Kumari, and S. Sudheer Khan, "Photocatalytic activation of CdS NPs under visible light for environmental cleanup and disinfection," *Sol. Energy*, vol. 105, pp. 542–547, Jul. 2014.

[12] X. Yang, B. Wang, Y. Mu, M. Zheng, and Y. Wang, "Photocatalytic Performance of Cubic and Hexagonal Phase CdS Synthesized via Different Cd Sources," *J. Electron. Mater.*, vol. 48, no. 5, pp. 2895–2901, May 2019.

[13] J. Yaseen, P. B. Sable, and G. M. Dharne, "Growth and Characterization of CdS Nanoparticles for Phtotovolatic Cell Application," 2018.

[14] H. Sivaram, D. Selvakumar, and R. Jayavel, "PVP capped CdS nanoparticles for UV-LED applications," in *AIP Conference Proceedings*, 2015, vol. 1665, no. 1, p. 050168.

[15] B. S. Rao, B. Rajesh Kumar, V. R. Reddy, and T. S. Rao, “PREPARATION AND CHARACTERIZATION OF CdS NANOPARTICLES BY CHEMICAL CO-PRECIPITATION TECHNIQUE,” 2011.

[16] V. Singh and P. Chauhan, “Structural and optical characterization of CdS nanoparticles prepared by chemical precipitation method,” *J. Phys. Chem. Solids*, vol. 70, no. 7, pp. 1074–1079, Jul. 2009.

[17] T. Lavanya and N. V. Jaya, “Synthesis and Characterization of Pure CdS Nanoparticles for Optoelectronic Applications,” *Trans. Indian Ceram. Soc.*, vol. 70, no. 3, pp. 119–123, Jul. 2011.

[18] G. Murali, D. Amaranatha Reddy, B. PoornaPrakash, R. P. Vijayalakshmi, B. K. Reddy, and R. Venugopal, “Room temperature magnetism of Fe doped CdS nanocrystals,” *Phys. B Condens. Matter*, vol. 407, no. 12, pp. 2084–2088, Jun. 2012.

[19] G. Giribabu, D. A. Reddy, G. Murali, and R. P. Vijayalakshmi, “Structural and optical studies on Mg doped CdS nanoparticles by simple co-precipitation method,” in *AIP Conference Proceedings*, 2013, vol. 1512, no. 1, pp. 186–187.

[20] H. Sekhar and D. N. Rao, “Spectroscopic studies on Fe 3+ doped CdS nanopowders prepared by simple coprecipitation method,” *J. Alloys Compd.*, vol. 517, pp. 103–110, Mar. 2012.

[21] N. H. Patel, M. P. Deshpande, and S. H. Chaki, “Study on structural, magnetic properties of undoped and Ni doped CdS nanoparticles,” *Mater. Sci. Semicond. Process.*, vol. 31, pp. 272–280, Mar. 2015.

[22] G. Giribabu, G. Murali, D. Amaranatha Reddy, C. Liu, and R. P. Vijayalakshmi, “Structural, optical and magnetic properties of Co doped CdS nanoparticles,” *J. Alloys Compd.*, vol. 581, pp. 363–368, Dec. 2013.

[23] H. Mikhail and F. I. Agami, “Magnetic susceptibility of group II, group VI semiconductors,” *J. Phys. Chem. Solids*, vol. 27, no. 6–7, pp. 909–912, Jun. 1966.

[24] F. Ibraheem *et al.*, “Tuning Paramagnetic effect of Co-Doped CdS diluted magnetic semiconductor quantum dots,” *J. Alloys Compd.*, vol. 834, p. 155196, Sep. 2020.